

RSC Advances



This is an *Accepted Manuscript*, which has been through the Royal Society of Chemistry peer review process and has been accepted for publication.

Accepted Manuscripts are published online shortly after acceptance, before technical editing, formatting and proof reading. Using this free service, authors can make their results available to the community, in citable form, before we publish the edited article. This *Accepted Manuscript* will be replaced by the edited, formatted and paginated article as soon as this is available.

You can find more information about *Accepted Manuscripts* in the [Information for Authors](#).

Please note that technical editing may introduce minor changes to the text and/or graphics, which may alter content. The journal's standard [Terms & Conditions](#) and the [Ethical guidelines](#) still apply. In no event shall the Royal Society of Chemistry be held responsible for any errors or omissions in this *Accepted Manuscript* or any consequences arising from the use of any information it contains.

Cite this: DOI: 10.1039/c0xx00000x

www.rsc.org/xxxxxx

ARTICLE TYPE

Nitroxide-coated Silver Nanoparticles: Synthesis, Surface Physicochemistry and Antibacterial Activity

Magdalena Gozdziwska,^a Grzegorz Cichowicz,^a Katarzyna Markowska,^b Katarzyna Zawada^c and Elżbieta Megiel^{a*}

Received (in XXX, XXX) Xth XXXXXXXXX 20XX, Accepted Xth XXXXXXXXX 20XX

DOI: 10.1039/b000000x

In this paper, we describe the facile synthesis and physicochemical characteristic of nitroxide-coated silver nanoparticles. The proposed procedure allows to obtain isolatable, devoid of Ag⁺ impurities, long-term stable, spherical nanoparticles with an average diameter ca. 7 nm, which exhibit high antibacterial activity towards both Gram-negative and Gram-positive strains. The determined Minimum Bactericidal Concentrations (MBCs) are significantly lower than the values reported for other thiolate-capped silver nanoparticles and range from 4 µg/ml (against *Pseudomonas aeruginosa*) to 12 µg/ml (against *Staphylococcus aureus*). Our studies proved that the nitroxide coverage favours antibacterial activity of silver nanoparticles, probably due to the ability of nitroxides to be oxidized by reactive oxygen species (ROS) to positively charged oxoammonium ions which can interact strongly with bacterial membrane. Furthermore, the mechanism of chemisorption of disulphide bisnitroxide on silver surface has been discussed on the basis of XPS, FTIR and ESR results.

1. Introduction

In recent years, silver nanoparticles (AgNPs) have been one of the most studied materials, because of their unique optical, catalytic, electrical and biological properties which cannot be observed in bulk silver.¹ First of all, AgNPs exhibit the intensive localized surface plasmon resonance (LSPR) which can be tuned to any wavelength in visible spectrum.^{2a-d} Owing to the fact that the plasmon peak position strongly depends on the shape and size of AgNPs, the dielectric constant of surrounding material and mutual interactions, silver nanoparticles can be successfully used for the fabrication of chemical and biochemical sensors,³ bioimaging devices⁴ and plasmon circuitry elements.⁵ Moreover, the nanosilver has found important applications in catalysis¹ and SERS detection.⁶ However, biocidal activity, toxicity for higher organisms and influence on environment of AgNPs, are especially broadly researched, due to the potential applications of these materials as novel antibacterial drugs, that could become an alternative to the antibiotics currently in use.^{7a-d} Owing to the broad-spectrum of biocidal properties, the nanosilver has found application as an additive to great number of consumer products such as cosmetics, clothes, disinfectant sprays, antiseptic coatings for electronic devices, household equipment and medical devices. Its annual worldwide production is estimated at about 320 tons.⁸ Nevertheless, the mechanism of antibacterial effect of AgNPs is

still not completely understood. It is suggested that silver nanoparticles show pleiotropic effect on bacterial cells. So far, the three main ways to explain the microbial toxicity of AgNPs have been proposed in literature: 1) release of Ag⁺ ions from the nanoparticle surface and their further intracellular reactions with proteins and DNA^{9a,b}, 2) physical damage of the bacterial cell wall and further penetration inside the cell, 3) generation of reactive oxygen species (ROS) as a consequence of the interaction of silver ions with enzymes in respiratory chain leading to oxidative stress.¹⁰ It has been demonstrated that AgNPs antimicrobial efficiency depends on their size¹¹, shape¹² and in large degree on the surface charge.¹³ Additionally, the kind of capping ligand, stability and presence of other components in the studied material are crucial for the correct assessment antimicrobial activity and toxicity of AgNPs. Most of the published studies consider biocidal activity of AgNPs protected by electrostatically linked ligands (i.e. citrate, ascorbate, gallic acid) and thereby stable only in solution, which means that they cannot be isolated in a solid state from the reaction mixture. Therefore, preparation of nanoparticles in such a way may makes their purification from unreacted silver salts, stabilizers and others reagents used in their synthesis questionable. The research of El Badawy *et al.*¹³ has revealed the importance of removal of impurities from AgNPs suspensions on the accurate evaluation their toxicity. It is worth to point out that the comprehensive

physicochemical characterization of electrostatically protected AgNPs cannot be carried out which makes it difficult to perform standardized assays on them.^{7b}

In contrast to the electrostatically protected silver nanoparticles, thiolate-capped ones can be repeatedly isolated from the solution and re-dissolved, they are long-term air stable and can be easily characterized in solid state.¹⁴ However, there are only a few reports showing a biocidal activity of thiolate-capped silver nanoparticles. Amato *et al.* have described a two-step protocol to produce thiolate-capped AgNPs based on the post-functionalization of citrate stabilized colloidal silver using cysteine and glutathione as the capping agents. The obtained glutathione-coated AgNPs proved to be stable under the physiological conditions (6.8 < pH < 7.4, in the presence of electrolyte) and exhibited antibacterial activity against *Escherichia coli* and *Staphylococcus aureus*, while the cysteine-coated AgNPs tend to aggregate under the same conditions.¹⁵ It was demonstrated later that the glutathione-capped AgNPs are capable of damaging *E. coli* cell membrane.¹⁶ The antibacterial activities of AgNPs coated with mixed monolayers of thiols have been reported.¹⁷ Graf *et al.*¹⁸ have demonstrated synthesis of thiolate-capped AgNPs using dimeric peptide containing disulphide group.

Nitroxides, which have found numerous important applications, are a diverse group of stable radicals, having >N-O• moiety, with unpaired delocalized electron shared between the nitrogen and oxygen atoms. Nitroxides are extensively used as oxidation catalysts for organic synthesis,^{19,20} mediators for controlled polymerization,²¹ spin probes for biochemical research,²² magnetic resonance imaging (MRI) contrast agents²³ and building blocks for the preparation of organic magnets.²⁴ Recently, therapeutic and clinical applications of nitroxides have attracted particular attention. Due to the ability to degrade superoxide and peroxide radicals, to inhibit Fenton reaction and to couple with free radicals, nitroxides may function as efficient antioxidant in biological systems.²⁵ The mechanism of superoxide radicals degradation by nitroxides involves their one-electron reversible oxidation to oxoammonium ions according to Eq. 1.



Further, oxoammonium ion may be reduced back to nitroxide according to Eq. 2.



Due to the possible reaction with ROS and, in this way creation of positively charged oxoammonium ions, nitroxides can be useful as AgNPs ligands for biocidal applications. The presence of positive charge of oxoammonium ions on silver surface should allow to increase the strength of interactions with negatively charged bacteria cell membranes leading to their easier damage, similarly to the phenomenon observed for other positively covered AgNPs.¹¹ On the other hand, nitroxide-coated silver nanoparticles (N-AgNPs) by reacting with ROS may cause the reduction of ROS biocidal activity but simultaneously they might contribute to the toxicity attenuation and therefore reduce the side effects of drugs based on AgNPs related to ROS generation.

To the best of our knowledge synthesis, physicochemical properties and biocidal activity of silver nanoparticles coated with nitroxide have not been reported yet.

Recently, our group has proposed one-phase and two-phase procedures for synthesis of thiolate-capped gold nanoparticles using disulphide bisnitroxide as the capping agent.^{26,27} Moreover, we have shown that the nitroxide-coated gold nanoparticles obtained in this way are efficient as mediators in a coupling reactions with free radicals.²⁸

In this work we describe the synthesis of nitroxide-coated silver nanoparticles (N-AgNPs), the physicochemical characteristic of the obtained material and their antibacterial activity against representatives of Gram-negative bacteria - *E. coli*, *Pseudomonas aeruginosa*, *Klebsiella pneumoniae* and Gram-positive strains *S. aureus*, *Staphylococcus epidermidis*.

2. Experimental

2.1. Materials

NaBH₄, AgNO₃ and all solvents have been purchased from Sigma-Aldrich and used as received. Bis(N-oxy-2,2,6,6-tetramethylpiperidyl)-4,5-dithiooctanoate (DiSS) has been synthesized according to the procedure described in the literature.²⁹ Milli-Q ultrapure water (resistivity 18.2 MΩ/cm) has been used.

For antibacterial tests 96-well polystyrene microtitre plates (Greiner bio-one) have been used. The microbial strains have been chosen from American Type Culture Collection (ATCC): *E. coli* 23546, *P. aeruginosa* 10145, *K. pneumoniae* 13886, *S. aureus* 29213, *S. epidermidis* 12228. Cultures have been grown in Mueller–Hinton broth (MH; Biocorp Poland).

2.2 Preparation of nitroxide coated silver nanoparticles (N-AgNPs)

As a typical procedure, 38 mg AgNO₃ (223 μmol) has been dissolved in 60 ml of dimethylformamide (DMF), the appropriate amount of DiSS (required to achieve the assumed Ag⁺: DiSS molar ratio (see Table 1)) was added and the mixture was stirred using magnetic stirrer for 30 minutes. In the case of synthesis of AR2HH(-5) sample, the mixture was stirred under a continuous stream of argon. Wherein, in the synthesis of samples AI2HH(+5), AI2HH(-5) and AR2HH(-5) the reaction mixture was cooled in an ice bath.

The freshly prepared solution of NaBH₄ in DMF (the applied molar ratios Ag⁺: NaBH₄ and solution concentrations are given in Table 1) was added slowly (dropping velocity is given in Table 1) using peristaltic pump (Thermo Fisher Scientific) under vigorous stirring. After the mixture turned from light orange through pale-yellow to dark brown, the solution was stirred for an appropriate period of time and at a suitable temperature (see Table 1).

Then, ultrapure water (100 ml) with small amount of NaCl was added to the reaction mixture and the resulting solution was sonicated for 1 minute and then centrifuged (10 min, 10 000 rpm, -5°C). The supernatant fluid was discarded and a brown precipitate was washed with ultra-pure water (4×100 ml). The absence of impurities and free ligand was confirmed by TLC. The obtained solid was dried under vacuum at 30°C. Finally, the grey, solid products, soluble in the most common organic polar solvents, e.g. methanol, acetone, DMF, tetrahydrofuran (THF),

dimethyl sulfoxide (DMSO), acetonitrile were obtained. The solutions of the obtained N-AgNPs were stable and no detectable changes of the SPR peak were observed even after several months (ESI Fig. S6†).

2.3 Techniques used in N-AgNPs characterization

Electron Spin Resonance (ESR) measurements have been carried out at room temperature in acetone solution with an X-band (9.3 GHz) using spectrometer Miniscope MS200 (Magnettech GmbH, Berlin, Germany). Modulation frequency was 100 kHz. Simulations were performed using the EasySpin package in Matlab.

X-ray photoelectron spectroscopy (XPS) measurements have been done using a VG ESCALAB 210 electron spectrometer equipped with monochromatic Al K α source (1486.6 eV) of radiation. XPS data were calibrated using the binding energy of C1s transition at 284.6 eV as the internal standard.

Thermogravimetric measurements (TG) have been performed under N $_2$ using DuPont 951 thermobalance (precision $\pm 0.4\%$; minimal mass 0.02 mg) coupled with a DuPont 9900 thermal analyzer (heating rate 5K/min).

Transmission Electron Microscopy (TEM) observations have been carried out using JEM 1400 JEOL Co. microscope, at 120 kV acceleration voltage. The samples had been obtained by casting the acetone solution of nanoparticles onto a carbon coated nickel microgrid (200 mesh) and air-dried overnight. SEM - EDS spectroscopy measurements were carried out with scanning electron microscope JEOL-JSM-5600 equipped with energy dispersive X-ray spectrometer OXFORD Link-ISIS-300.

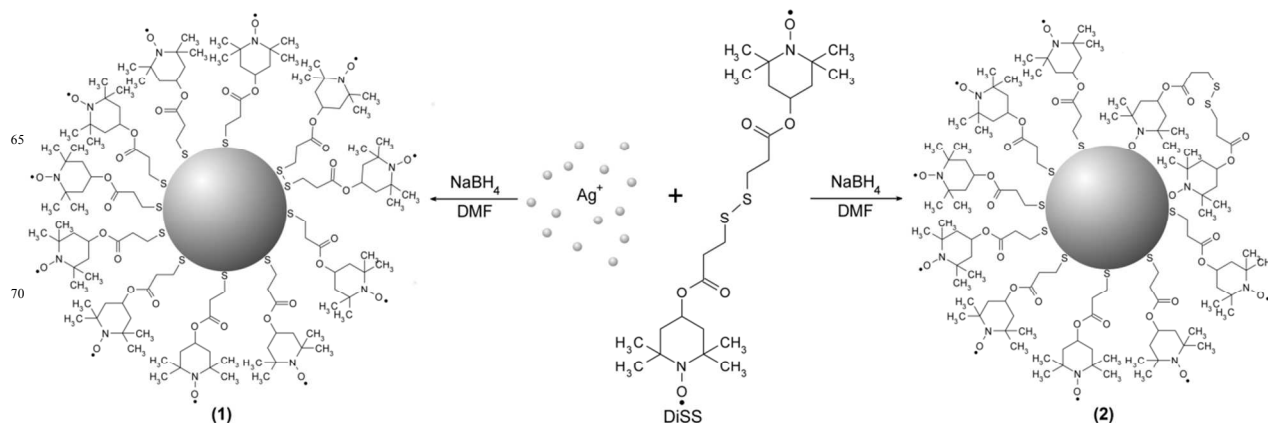
Fourier transform infrared (FTIR) spectroscopy has been performed on a Shimadzu FT-IR model 8400S

spectrophotometer. FTIR spectra (absorption mode) were recorded with resolution 4 cm $^{-1}$ from KBr pellets in a ratio of 1:1000 (w/w) in the case of N-AgNPs and 1:300 (w/w) for the capping ligand (DiSS).

Dynamic Light Scattering (DLS) measurements have been performed with Zetasizer Nano series apparatus (Malvern) with laser He-Ne (4 mW) at 632.8 nm.

UV-vis spectra have been recorded using a Cary 50 Conc UV-vis spectrophotometer.

Antibacterial activity measurements have been performed by determination of Minimum Inhibitory Concentrations (MICs) of N-AgNPs samples using the broth microdilution technique performed in 96-well microtitre plates according to CLSI standards.³⁰ Briefly, stock solution of N-AgNPs (1.6 mg/ml) were prepared by dissolving them in DMSO. A series of twofold dilutions of N-AgNPs in MH broth forming the range from 1 to 128 $\mu\text{g/ml}$ were obtained. Probes were then inoculated with tested bacterial cultures providing final cell density of 1×10^6 CFU/ml (CFU, Colony Forming Units). Plates were incubated statically at 37°C for 24 h. The lowest concentration of each tested N-AgNPs that resulted in no visible turbidity was considered as the MIC. As a control sample the solution of the highest used concentration of DMSO (4% v/v) or DiSS (128 $\mu\text{g/ml}$) was used. To determine the Minimum Bactericidal Concentrations (MBCs) residues from microtiter plate wells corresponding to determined MIC values and higher concentrations were spread onto MH agar Petri plates. The MBC was determined as the lowest concentration of N-AgNPs that reduced the bacterial viability by $\geq 99.9\%$. Each MIC and MBC determination was performed in triplicate.



Scheme 1. Synthetic route and two proposed structures of N-AgNPs.

3. Results and discussion

N-AgNPs have been synthesized by using one-phase procedure with AgNO $_3$ as a silver ions precursor, DiSS as stabilizer, DMF as reaction medium and solvent for reducing agent (NaBH $_4$) according to Scheme 1.

Table 1 summarizes the effects of the reaction conditions (a molar ratio of Ag $^+$ to NaBH $_4$, a molar ratio of Ag $^+$ to DiSS, reaction temperature, NaBH $_4$ dropping velocity, its concentration in DMF and kind of environment (air or argon) on the synthesis

of N-AgNPs. The first attempts at N-AgNPs synthesis have been based on the procedure, recently developed by our group,²⁶⁻²⁸ for the preparation of gold nanoparticles stabilized with nitroxides.

However, proceeding according to this protocol led to aggregation during the synthesis (see Table 1, sample 1). The most likely reason is that thiolate-stabilized AgNPs are not stable in alkaline solution and precipitated as a result of the aggregation.

Therefore, we have decided to decrease the amount of added NaBH $_4$ to avoid nanoparticles precipitation from the solution at pH > 7. The stable product has been obtained when the ratio of Ag $^+$ to NaBH $_4$ was changed from 1:10 to 1:1.25. Besides, our

studies proved that the lowering of NaBH_4 concentration in DMF as well as its dropping velocity to the reaction mixture and lowering of reaction temperature improved size distribution of the obtained silver nanoparticles. The decrease in reaction temperature was limited to -5°C due to the low solubility of the ligand (DiSS) below this temperature. Also, we observed, that the optimal time of reaction is 2 hours because after this time product begins to gradually aggregate, partially precipitating itself from the solution. It is clearly visible as a decrease of intensity of surface plasmon resonance after 2 h of reaction (ESI Fig. S7†). Further, when the reaction is performed under argon atmosphere,

instead of the air, contribution of larger particles in the obtained material is significantly lower (see sample AI2HH(-5) and AR2HH(-5) in Fig.1). Fig. 1 shows TEM images of the obtained nanoparticles in the order of gradual improvement of reaction conditions. It is clearly visible that of all the studied conditions, these applied in synthesis of sample AR2HH(-5) are optimal and allow to obtain spherical and nearly uniformly distributed nanoparticles.

Fig. 2 displays a histogram of size distribution of nanoparticles in the sample AR2HH(-5) obtained on the basis of TEM image.

Table 1 Effects of reaction conditions on N-AgNPs synthesis.

Sample	$\text{Ag}^+ : \text{DiSS}$ ratio	$\text{Ag}^+ : \text{NaBH}_4$ ratio	Reaction temperature [$^\circ\text{C}$]	Environment	Concentration of NaBH_4 [mg/ml]	Reaction time [h]	Dropping velocity [ml/min]	Yield [%] ^a
(1)	1:0.5	1:10	RT	Air	5.8	24	3.0	Aggregation
(2)	1:0.5	1:5	RT	Air	2.9	24	3.0	Aggregation
(3)	1:0.5	1:4	RT	Air	2.3	2	3.0	Aggregation
(4)	1:0.5	1:3	RT	Air	1.75	24	3.0	Not stable
AI24RT	1:0.7	1:1.25	RT	Air	1	24	0.5	18
AI24RTH	1:0.6	1:1.75	RT	Air	1.2	24	0.6	16
AI2HH(+5)	1:1	1:1.75	+5	Air	0.6	2	0.8	59
AI2HH(-5)	1:1	1:1.75	-5	Air	0.6	2	0.8	61
AR2HH(-5)	1:1	1:1.75	-5	Argon	0.6	2	0.8	57

^a calculated on the basis of content of silver determined from TG analysis (see Fig. 9).

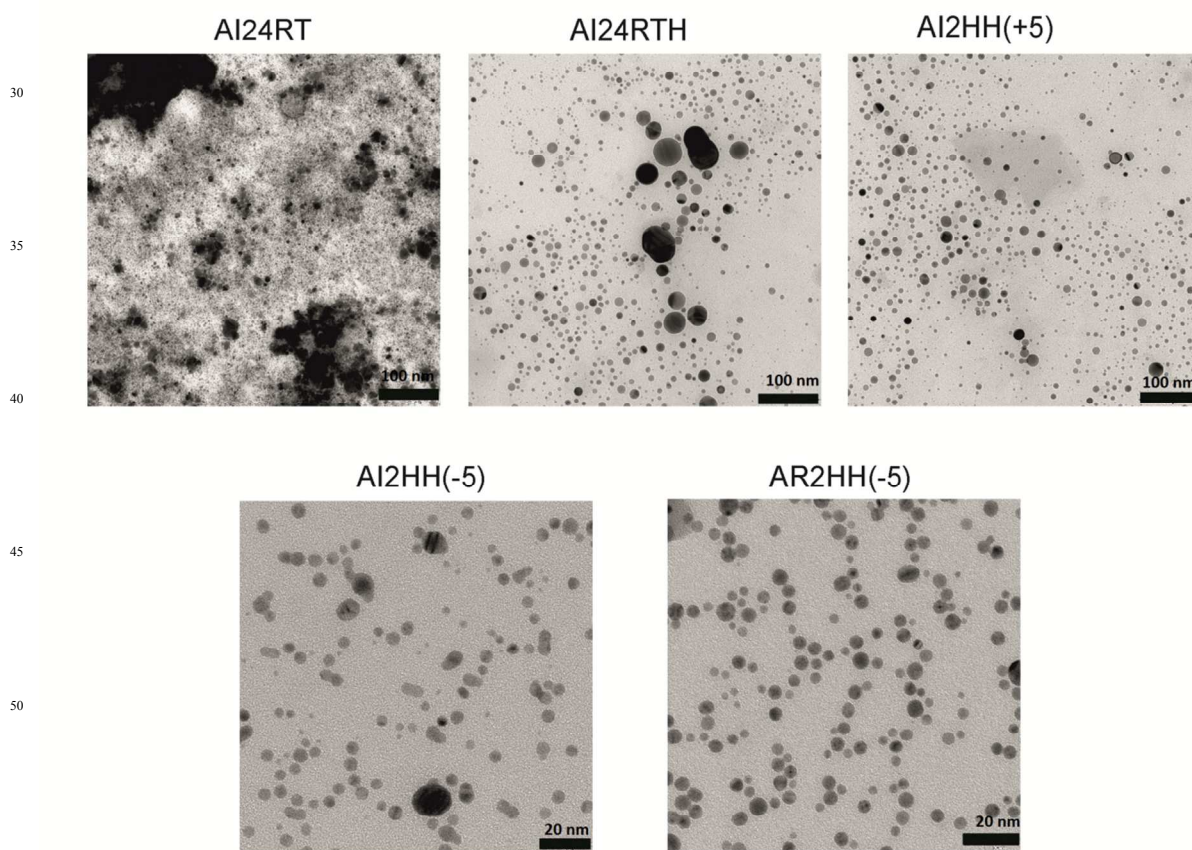


Fig. 1 TEM images of the synthesized N-AgNPs.

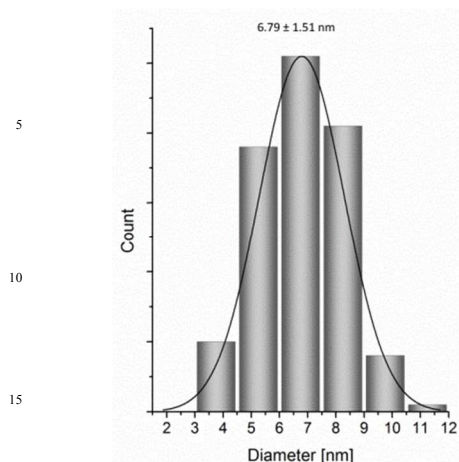


Fig. 2 Size distribution histogram of N-AgNPs in the sample AR2HH(-5) prepared on the basis of TEM image (see Fig. 1).

Fig. 3 shows UV-vis spectra of N-AgNPs obtained under different reaction conditions (see Table 1). For all samples the surface plasmon resonance (SPR) band, typical for spherical silver nanoparticles, has been observed, but with different value of full width at half maximum (FWHM) and wavelength of maximum absorption (λ_{max}). Considering the FWHM and λ_{max} of absorbance curves in Fig.3 we can compare polydispersity and the average size of nanoparticles in the studied samples. These findings are consistent with the results obtained from TEM analysis. For instance, according to TEM images, the sample AI24RT contains the biggest particles and even aggregates (see Fig.1) and, as could be expected, the maximum of SPR occurred at the longest wavelength (Fig.3). For the sample AI2HH(-5) containing smaller nanoparticles with significant narrower polydispersity λ_{max} is the same, however FWHM is significantly lower. The most symmetric absorption curve with the lowest FWHM and the lowest λ_{max} was recorded for the sample AR2HH(-5) which confirms that the reaction conditions, applied in this case, were optimal. Further, UV-vis spectra showed a lack of the band at ca. 350 nm associated with Ag^+ -thiolate complex,³¹ which clearly demonstrates that the obtained products are devoid of Ag^+ impurities.

Fig. S8† in ESI shows the average hydrodynamic diameters of the synthesized N-AgNPs obtained on the basis of DLS measurements performed for the same solutions for which UV-vis spectra have been recorded. The findings from DLS measurements confirmed earlier conclusions concerning influence of the reaction conditions on the polydispersity of the obtained nanoparticles.

It is also worth noting that, as can be seen in the TEM image of sample AR2HH(-5) in Fig. 1, the obtained spin-coated silver nanoparticles exhibit tendency to self-organization in chainlike two-dimensional (2D) assembly on carbon-coated TEM grid.

Recently, we have reported similar phenomenon for gold nanoparticles with comparable size, covered with the same protecting ligand.²⁸

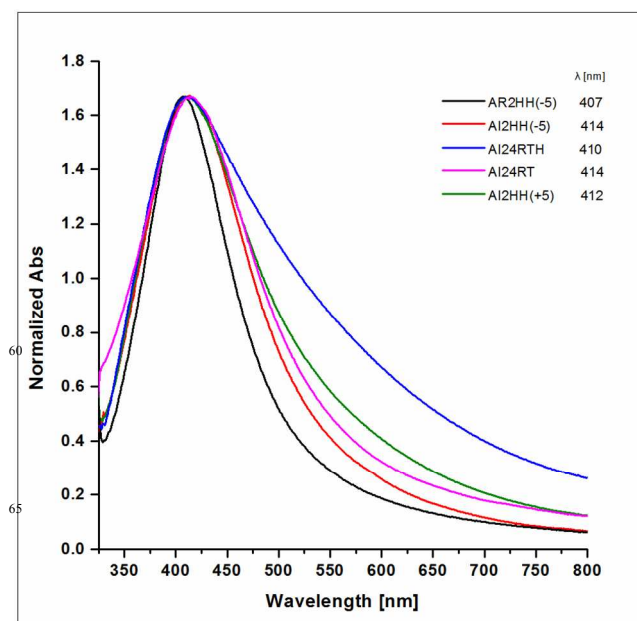


Fig. 3 UV-vis spectra of the obtained N-AgNPs in acetone solutions

Korgel *et al.* have shown that the hydrophobic dodecanthiol-capped silver nanocrystals can be organized into close-packed 2D lattices by solvent evaporating on carbon-coated TEM grid due to the attraction forces induced by highly polarizable nanosilver core.³²

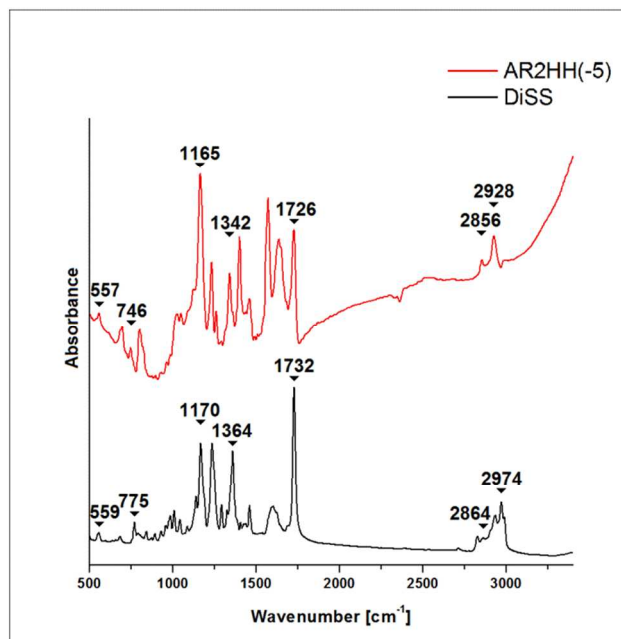


Fig. 4 FTIR spectra: synthesized N-AgNPs (sample AR2HH(-5)) and capping ligand (DiSS) used in the synthesis.

Fig. 4 shows FTIR spectra of N-AgNPs and capping ligand used in the synthesis. The characteristic modes corresponding to the functional groups in the ligand molecule appear in N-AgNPs spectrum with maxima shifted to a lower wavenumber suggesting

that the molecular motions of molecules adsorbed on the silver surface are constrained. It is particularly visible for the modes of terminal groups such as the mode of nitroxyl moiety $>\text{NO}\bullet$ shifted from 1364 cm^{-1} to 1342 cm^{-1} and asymmetric stretching mode of the methyl groups in piperidine ring $\nu_a(\text{CH}_3)$ that is shifted from 2974 cm^{-1} to 2928 cm^{-1} (position of symmetric mode of CH_3 group cannot be determined due to the signal broadening). The symmetric stretching mode of methylene groups $\nu_s(\text{CH}_2)$ appears at 2856 cm^{-1} and at 2864 cm^{-1} in nanoparticles spectrum and in ligand spectrum, respectively (position of asymmetric mode of CH_2 group cannot be determined due to the signal broadening). The significant shifting of $\nu_s(\text{CH}_2)$ band to a lower wavenumber in N-AgNPs spectrum indicates that the molecular motions of the moieties directly attached to the silver surface are constrained. It is worth mentioning that the position of the methylene mode $\nu_s(\text{CH}_2)$ in the FTIR spectrum of N-AgNPs is similar to the position of this band observed in the FTIR spectra of solid thiols in crystalline phase and in the spectra recorded for crystalline-like self-assembled monolayers (SAM) created by thiols adsorbed on gold surface.³³ These data indicate that the nitroxide species adsorbed on the nanosilver surface in the synthesized nanoparticles are ordered in a self-assembled monolayer due to the intermolecular forces. The same forces may be responsible for the tendency of N-AgNPs to form chainlike 2D assembly.

The remaining peaks maxima in the FTIR spectrum of N-AgNPs are slightly shifted to a lower wavenumber, for instance, the band corresponding to $\text{C}=\text{O}$ mode is shifted from 1732 cm^{-1} to 1726 cm^{-1} , the mode of $-\text{C}-\text{O}-$ group from the ester moiety from 1170 cm^{-1} to 1165 cm^{-1} which probably indicates that in further distance from the surface organic layer is less close-packed. Note that the band corresponding to the disulphide mode is present not only in DiSS spectrum (at 559 cm^{-1}) but also slightly shifted in nanoparticles spectrum (at 557 cm^{-1}), which will be discussed later. The most significant shift of position of nitroxyl mode observed in FTIR spectrum of N-AgNPs in comparison with ligand spectrum may indicate strong interactions between radicals depending on the spin density delocalization.³⁴ In order to verify this hypothesis we have carefully analysed the ESR spectra of the obtained N-AgNPs. As it turned out, the ESR spectra of the obtained nanoparticles, shown in Fig. 5, are a result of superposition of three components, namely broad singlet, triplet and quintet signal, as shown in Fig. 6 for the AR2HH(-5) sample. The contribution of each component, as obtained from simulations, is shown in Table 2.

Table 2 The contribution of ESR spectra components to total intensity (%) and broad singlet linewidth.

Sample	Triplet	Broad line (singlet)	Quintet	Singlet linewidth [mT]
AI24RT	57.0	33.2	9.8	2.60
AI24RTH	29.2	57.5	5.7	1.91
AI2HH(+5)	22.5	64.7	12.9	1.75
AI2HH(-5)	22.5	68.6	8.9	1.89
AR2HH(-5)	22.1	62.1	15.8	1.62

As can be seen, in most cases, i.e. for samples AI24RTH,

AI2HH(+5), AI2HH(-5) and AR2HH(-5), the largest contribution to the total signal intensity is from the broad singlet component, resulting from the averaging of signals from spin-spin interacting radicals with a wide distribution of coupling constants J .³⁵

The domination of such a broad single signal has been reported by Chechik *et al.*³⁶ for thiolate-capped gold nanoparticles with high concentration of nitroxides attached to the gold surface, and it was also observed in our earlier work for nitroxide-modified gold nanoparticles.^{26,27}

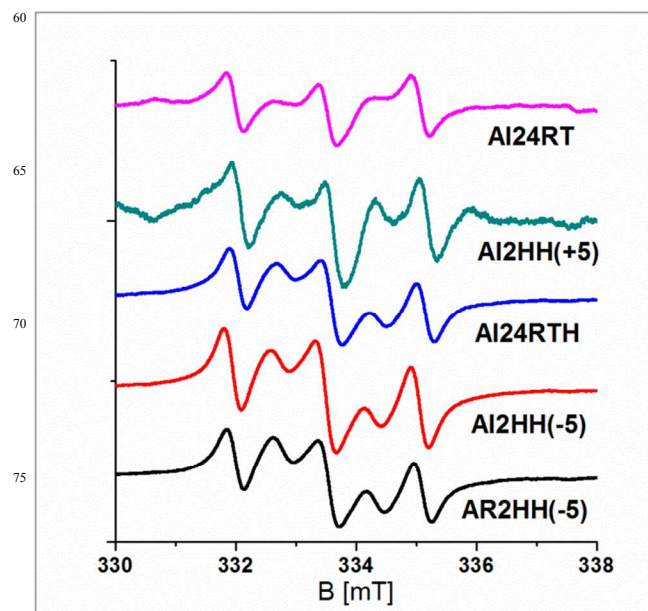


Fig. 5 ESR spectra of the obtained N-AgNPs in acetone solution at 293 K.

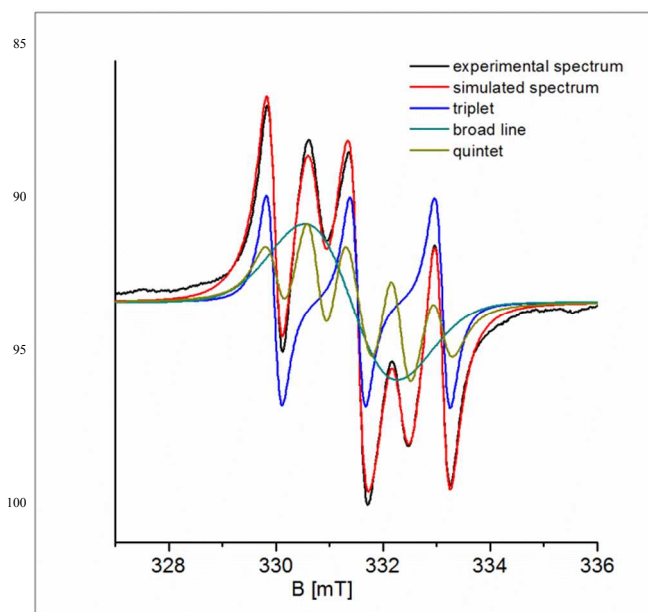


Fig. 6 ESR spectrum of N-AgNPs (sample AR2HH(-5) in acetone solution at 293 K) and simulated components of this spectrum.

The superiority of the broad line component indicates relatively

high surface coverage, with some distribution of inter-nitroxide distances, as J depends on distance between interacting spins.³⁷ In case of N-AgNPs obtained in this work, the linewidth of this component (peak-to-peak line width 1.62-2.6 mT, as shown in Table 2, with the smallest value for AR2HH(-5) sample is comparable to values reported by Chechik *et al.*³⁶ for thiolate-capped gold particles with different number of nitroxide spin probes per nanoparticle (from 10 to 60, with linewidths from 2.48 to 1.62 mT, respectively), and is larger than the one observed for gold nanoparticles functionalized with the same binitroxide disulphide (1.6 mT).²⁶ As the linewidth increases with decreasing nitroxide:nanoparticle ratio, it can be suggested that either average interactions between nitroxides adsorbed on silver nanoparticles are weaker than between these adsorbed on gold nanoparticles or the coverage of silver nanoparticles is lower. In case of AI24RT sample the ESR spectrum is dominated by triplet component, which accounts for almost 60% of total intensity. In the ESR spectrum of other samples it accounts for 22.1-29.2% of total intensity. This signal with an isotropic ¹⁴N-hyperfine splitting of 1.575 mT is probably due to isolated adsorbed radicals, as such signals are obtained for nitroxide radicals in solution in non-polar local environment.^{38,39} As the contribution of the triplet component to the total intensity of ESR spectra is larger than in the case of gold nanoparticles coated with the same nitroxide radical, it would support the hypothesis of generally lower coverage of the silver nanoparticles with nitroxides when compared with the gold ones. The domination of the triplet component in the ESR spectrum of AI24RT sample suggests large spatial distribution among nitroxides in this sample, as similar signal has dominated also in the ESR spectra of thiolate-capped gold nanoparticles when long-chain nitroxide spin probe was used,³⁷ i.e. with no restriction of molecular motion, or in our earlier work for small nitroxide-modified gold nanoparticles (average diameter 2.25 nm).²⁷ It can be expected that, as in case of gold nanoparticles, the adsorption of disulphides on silver nanoparticles proceeds also independently for both branches.⁴⁰ However, the hyperfine splitting constant is slightly larger in case of the silver nanoparticles than in case of gold ones (1.575 vs 1.54 mT),²⁶ suggesting the influence of metal core. It could be due to the different energy of surface plasmons in silver and gold nanoparticles. As for the contribution of a quintet component, it varies from 5.7 to 15.8% of total intensity. This component arises from strongly interacting pairs of nitroxide radicals, with $J \gg a_N$, although this interaction is not entirely due to exchange coupling, since the intensity ratio of five lines is not equal to 1:2:3:1. Still, the presence of quintet component suggests the presence of significant population of radicals adsorbed in close proximity to each other, in contrast to radical pairs giving rise to broad singlet signal. A similar component was observed for tetraoctylammonium bromide-capped gold nanoparticles labelled with 2,2,6,6-tetramethylpiperidine-1-oxyl radical (TEMPO) derived nitroxides, where it was responsible for less than 1% of total intensity,²⁶ but it was not observed for the gold nanoparticles covered solely with nitroxides.²⁸ Therefore, it seems that in systems obtained in this work there is a significant amount of strongly interacting radicals. Combined with the above-mentioned increase in linewidth of the singlet signal, as compared with the gold nanoparticles coated with nitroxides, it is an

additional support for the hypothesis of lower nanoparticle coverage of silver nanoparticles versus gold ones, but with stronger average interactions between radicals.

N-AgNPs (sample AR2HH(-5)) were further characterized by X-ray photoelectron spectroscopy (XPS) and the results were compared with the XPS spectra of capping ligand used in the synthesis to provide the detailed information on chemical composition of the surface and the mechanism of the ligand attachment to the nanoparticle surface. The quantitative data from the XPS analysis of N-AgNPs are presented in Table 3 (for capping ligand see Table S2 in ESI†).

Table 3 Binding Energy Values, full width at half maximum (FWHM) of peaks and atomic concentrations derived from XPS analysis of N-AgNPs (sample AR2HH(-5)).

Orbital	Position [eV]	FWHM [eV]	Concentration [atom %]
Ag 3d _{5/2}	368.4	0.980	13.6
	370.9	1.503	0.56
Ag 3d _{3/2}	374.4	0.980	9.27
	377.0	1.503	0.38
N 1s	399.2	1.221	1.20
	400.6	1.221	1.20
	402.2	1.221	0.50
O 1s	530.9	1.353	0.60
	532.4	1.353	9.30
	533.5	1.353	3.70
S 2p _{3/2}	161.9	1.448	1.40
	163.7	1.181	0.30
S 2p _{1/2}	163.1	1.448	0.70
	164.9	1.181	0.10
C 1s	285.0	1.341	34.3
	285.8	1.341	8.60
	286.8	1.341	5.70
	289.0	1.341	3.20

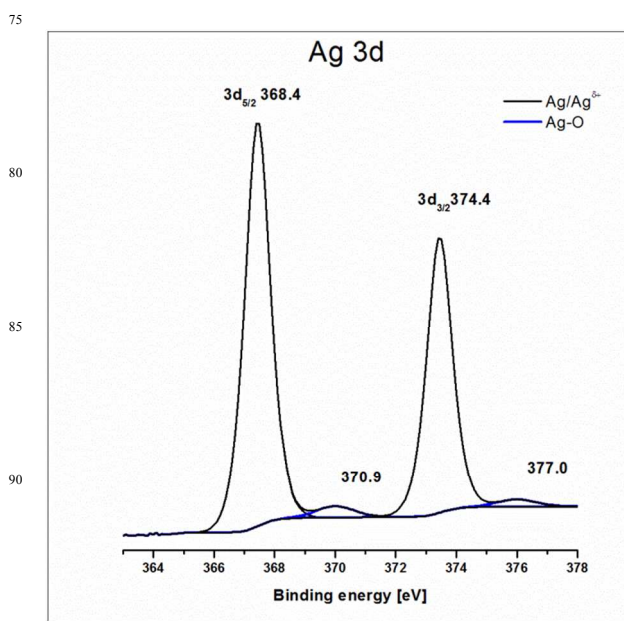


Fig. 7 XPS spectrum Ag3d of N-AgNPs (sample AR2HH(-5)).

The Ag3d spectrum of the obtained nanoparticles, as shown in Fig.7, consists of two main peaks centred at 368.4 eV and 374.4 eV corresponding to the binding energies of 3d_{5/2} and 3d_{3/2} orbitals, respectively with typical for AgNPs ascertained splitting of 3d doublet equal to 6 eV.⁴¹

The determined binding energies (BDEs) of 3d orbitals are very slightly shifted to higher energies in comparison with zero-valent silver (368.2 eV for 3d_{5/2} and 374.2 eV for 3d_{3/2})⁴² and they are comparable to those reported for AgNPs similar in shape and size, supported on high ordered graphite (HOPG).⁴³ It is worth mentioning that the outer silver atoms in the nanoparticles should be oxidized upon thiolate bond formation, thus it may be expected that the position of obtained signals should be shifted to higher binding energies. In practice, only slight changes have been observed since the obtained signals are a result of charge averaging of zero-valent and oxidized silver atoms in the sample

(Ag/Ag^{δ+}). Additionally, in the Ag3d spectrum region two bands at 370.9 eV and 377 eV with high value of FWHM (1.5 eV) were found. These signals were unambiguously assigned to 3d_{5/2} and 3d_{3/2} orbitals of the silver atoms bounded to oxygen atoms.⁴¹

The ratio of the area of the signal at a lower binding energy to that at a higher, for each of orbitals, gives a value of 24 which corresponds to about 4% of silver atoms bonded to oxygen atoms. It has been reported that the molecular oxygen adsorbed on the silver surface causes opposite shifting (negative) of Ag3d signals.⁴⁴ Negative shifting is more prominent in the case of ionic Ag-O bonds for example in silver oxides Ag₂O and AgO (367.3 eV and 373.6 eV for 3d_{5/2} and 3d_{3/2} orbitals respectively).⁴⁵ Thus observed by us positively shifted additional peaks assigned to Ag3d orbitals may indicate the presence of Ag-O bonds with a more covalent character.

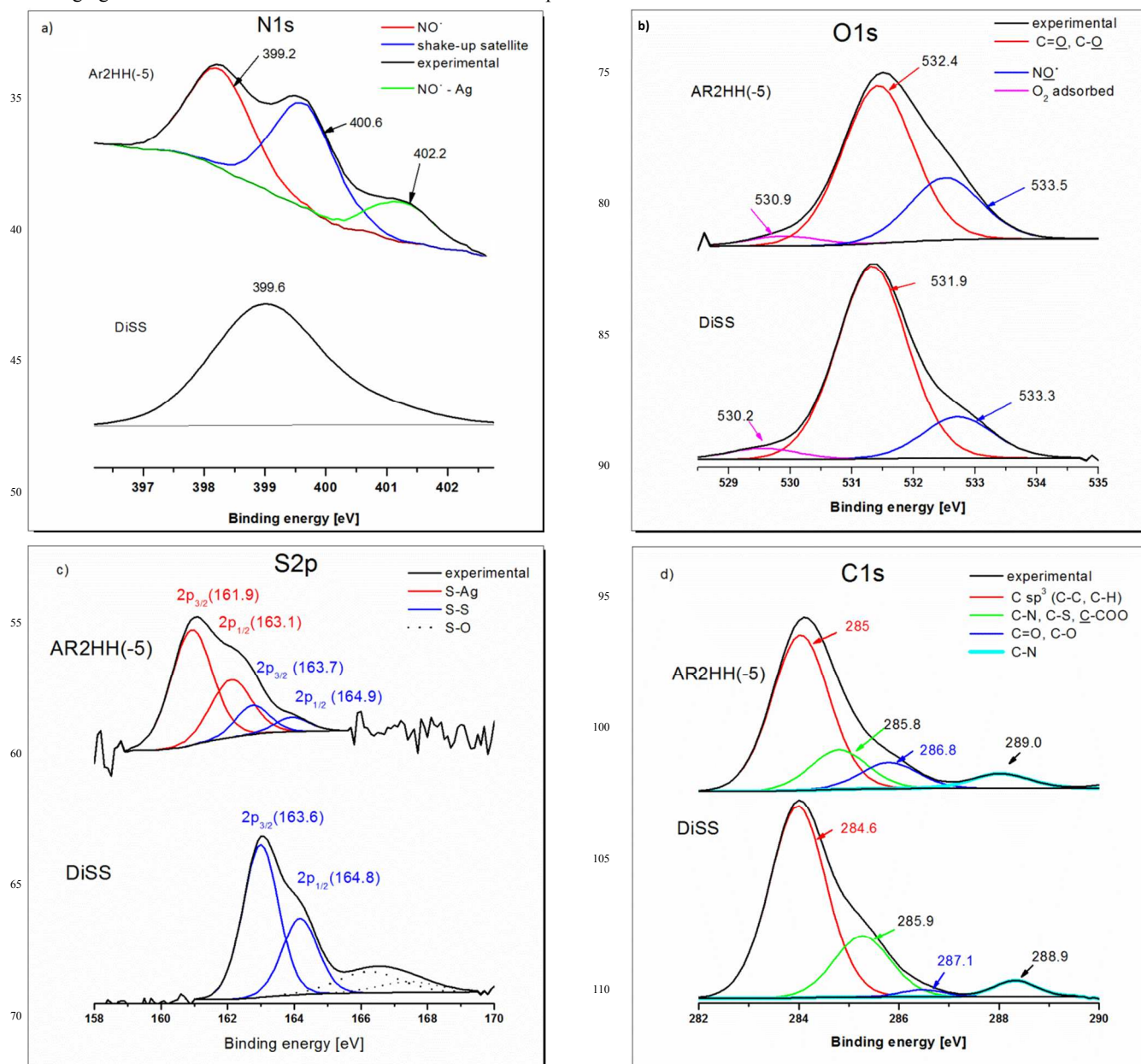


Fig. 8 XPS spectra of N-AgNPs (sample AR2HH(-5)) and the capping-ligand (DiSS). The calibrated values of BDE are presented.

Cite this: DOI: 10.1039/c0xx00000x

www.rsc.org/xxxxxx

ARTICLE TYPE

In our opinion such type of Ag-O bond can be formed between unpaired electrons of nitroxides and conduction electrons from the silver surface. Our group has recently demonstrated that the nitroxide radicals can be successfully attached to the gold surface by means of Au-O bonds.⁴⁶ It seems highly probable that the silver atoms may also form similar bonds with nitroxide radicals. However, it is worth noting that the formation of Ag-O bonds on AgNPs surface must result in a lower coverage of silver surface in comparison with only thiolate-capped AgNPs due to the steric effects associated with the presence of inversely orientated ligands (see structure **(2)** in Scheme 1). Indeed, our current ESR studies suggest a lower radical coverage of N-AgNPs in comparison with the gold nanoparticles coated with nitroxide studied earlier (see discussion above). Also, in the case of gold nanoparticles synthesized using the same capping-ligand the contribution of Au-O bonds has not been observed in XPS spectra.²⁷

The obtained XPS spectrum of N1s orbital of N-AgNPs provides further support for our hypothesis of Ag-O bonds formation between nitroxide radicals and nanoparticles surface. As can be seen in Fig. 8a, N1s spectrum of N-AgNPs is significantly broader than the N 1s spectrum of capping-ligand (DiSS).

The N1s spectrum of N-AgNPs can be deconvoluted into three peaks at 399.2 eV, 400.6 eV and 402.2 eV all with FWHM = 1.2 eV. First two components are very similar to those observed in N1s spectrum of nitroxide-coated gold nanoparticles (399.2 eV, 401.1 eV)²⁷ and have been attributed to the nitrogen of nitroxide group NO• and shake-up satellite, respectively. The latter, satellite peak had been observed earlier for thin films of nitroxide derivatives placed on the solid support,⁴⁷ while, the third observed in N1s spectrum peak, significantly shifted to a higher binding energies (at 402.2 eV), may be assigned to the nitrogen of nitroxide group attached to nanoparticle surface via Ag-O bond. Castro *et al.*⁴⁸ have reported N1s XPS spectrum for azomethane adsorbed on Ag(111) surface via interactions between nitrogen atoms and low-energy silver electrons at very similar position (402.1 eV). Obviously, the interactions between >NO• bonds and silver surface should also be visible in O1s XPS spectrum. However, O1s spectra of N-AgNPs and capping ligand (see Fig. 8b) do not differ significantly. The band attributed to the oxygen atom in the nitroxide group is centered at 533.3 eV (FWHM=1.33 eV) in case of ligand and at 533.5 eV (FWHM=1.35 eV) for N-AgNPs. A slight shifting and slight broadening of this component of O1s spectrum cannot be taken as evidence for the presence of Ag-O bonds.

The XPS spectrum of S2p of N-AgNPs and capping ligand have been shown in Fig. 8c. The broad spectrum of S2p of N-AgNPs was deconvoluted into four peaks corresponding to orbitals 2p_{3/2} and 2p_{1/2} in two different chemical environments. This demonstrates the presence of two sulphur species in organic layer adsorbed on the silver surface. The fitted peaks at 161.9 eV and 163.1 eV, which do not appear in the case of ligand spectrum, are unambiguously assigned to 2p_{3/2} and 2p_{1/2} orbitals of sulphur

thiolate bound to the silver surface.^{49,50} Whereas the signals at 163.7 eV and 164.9 eV correspond most likely to 2p_{3/2} 2p_{1/2} orbitals of still intact disulphide bonds which is consistent with the disulphide signals positions in the ligand spectrum (163.6 eV and 164.8 eV) and literature data for disulphides (163.9 eV and 165.1 eV).⁴¹ The FTIR spectrum of N-AgNPs (see Fig.4) evidently confirmed the presence of disulphide bonds in the protecting organic layer on the nanoparticles surface (a characteristic S-S stretching band appears at 557 cm⁻¹). It is intriguing, however, that in case of gold nanoparticles which were synthesized using the same capping ligand in our lab, organic layer on the gold surface did not contain disulphide molecules (it was demonstrated by XPS and FTIR analyses).^{26,27} Besides, the mechanism of chemisorption of disulphides on gold and silver surface, based on the sulphur-sulphur bond cleavage in two separate thiolate moieties, is the most commonly recognized one.^{40,47,51} On the other hand, the presence of intact disulphide bonds in organic layer on silver nanoparticles surface was also reported.^{18,52} Our quantitative XPS results (presented in Table 3) show that during the chemisorption process ca. 80% of disulphide bonds are cleaved and attached to the resulting monoradicals are attached to the silver surface as thiolate moieties (ca. 20% of sulphur atoms is bonded in disulphide groups). We think that the remaining DiSS ligands may be linked to nanoparticle by disulphide groups adsorbed on the surface (see structure **(1)** in Scheme 1) or by Ag-O bonds (see structure **(2)** in Scheme 1). On the basis of the ratio of the area of signals attributed to sulphur of S-S bonds to the total area of all four peaks in XPS S2p spectrum it may be evaluated that about 1 per 10 ligands is linked via one of the proposed two ways and not through a thiolate sulphur atom. The presence of nanoparticles with the structure **(1)** in the studied material could be responsible for the quintet contribution in the recorded ESR spectra. As was discussed earlier, this kind of contribution to ESR spectrum is related to the presence of radicals adsorbed in close proximity to each other. According to the theoretical simulations of the experimental ESR spectrum of AR2HH(-5) sample, the contribution of quintet component is ca. 16% what would correspond to biradicals amounting to ca. 8% of all ligands attached to the surface (see structure **(1)** in Scheme 1). Taking into account that the global number of ligands containing disulphide bonds represents ca. 10% of total ligand population it may be estimated that ca. 1-2% of ligands may be linked by Ag-O bonds (see structure **(2)** in Scheme 1).

It is also worth mentioning that the N-AgNPs obtained under argon atmosphere, in the contrary to capping ligand used in synthesis, do not contain oxidized sulphur (see Fig. 8c).

The obtained XPS spectrum of C1s orbital of N-AgNPs also confirmed the functionalization of silver surface with nitroxide radical used in the synthesis. As can be seen in Fig. 8d the fitted experimental spectra of N-AgNPs and DiSS may be deconvoluted into four peaks which maxima are very close in both spectra and can be assigned to the following groups: sp³ carbon atoms at 285 eV for N-AgNPs, 284.6 eV for DiSS (literature data 285.2 eV)⁵³,

C-N bonds in piperidine ring at 285.8 eV and 289.0 eV for nanoparticles and 285.9 eV, 288.9 eV for DiSS (literature data 285.2 eV and 289.2 eV, respectively),⁵⁴ C=O and C-O- groups in ester-group at 286.8 eV for N-AgNPs, 287.1 eV for DiSS (literature data 287.0 eV).⁵⁵

The grafting density of nitroxides on the silver nanoparticles surface has been determined by thermogravimetric analysis (TGA) and XPS. Results of quantitative determination of ligand (DiSS) density on idealized spherical nanoparticles with diameter of 7 nm (see Fig.1 and Fig.2), are shown in Table 4 (for the details on the calculations procedure see ESI†).

Table 4 The surface density of ligand molecules (DiSS) on the obtained N-AgNPs (sample AR2HH(-5)) calculated from TGA and XPS measurements (the estimated error limits: ± 1.4 molecules/nm² and $\pm 2.4 \times 10^{-10}$ [mol/cm²]).

Grafting density σ	From TGA	From XPS			
		S/Ag	N/Ag	C/Ag	O/Ag
[molecules/nm ²]	3.5	3.6	4.0	6.2	6.5
[mol/cm ²] $\times 10^{-10}$	5.8	6.0	6.6	10	11

It is well-known that TGA yields an organic weight fraction for the nanoparticles and can be successfully used for quantitative determination of their surface coverage.⁵⁶ The determined surface density of DiSS from TGA measurements equals 3.5 molecules/nm² and corresponds to 7 nitroxide-functionalized thiolate ligands per nm². This value agrees very well with the value reported for gold nanoparticles covered with monolayer of thiols (e.g. 6.26 ± 0.59 nm⁻² for gold nanoparticles capped with 3-mercaptopropionic acid).⁵⁷ As can be seen in Table 4 surface coverage determined from TGA is consistent with the values calculated from the XPS sulphur/silver and nitrogen/silver atomic

ratios. Whereas, the XPS carbon/silver and oxygen/silver atomic ratios indicate a greater packing density. Very recently, Torrelli *et al.*⁵⁸ have proven that the gold nanoparticles films yield an unrealistically high XPS carbon/gold atomic ratio through the attenuation of metal XPS signal and simultaneous enhancement of carbon XPS signal on increased curvature of the nanoparticles. Authors showed that the effect of attenuation of metal XPS signal is particular evident for nanoparticles of diameters below 20 nm. In our opinion, such an effect should be observed for similarly sized silver nanoparticles and can lead to significant overestimation of ligand density obtained on the basis of C/Ag atomic ratio. Likewise, the density of ligands on the synthesized N-AgNPs, determined on the basis of O/Ag atomic ratio, seems overestimated in comparison with the results from TGA and literature data. On the other hand, it is intriguing that the grafting density determined from TGA and from XPS using S/Ag and N/Ag atomic ratios are in very good agreement. It seems likely that the effect of enhancement of XPS signal is more clearly visible for elements for which atomic contribution in the ligand molecule is higher.

As was discussed earlier, due to the possible reaction of nitroxides with ROS and, in this way, creation of positively charged oxoammonium ions, N-AgNPs may exhibit enhanced antibacterial activity. Precise broth microdilution assays have been performed for several Gram-positive and Gram-negative bacteria, mostly pathogens. The obtained results are presented in Table 5. Determined MIC values confirmed that all of the studied N-AgNPs samples exhibit antimicrobial activity.

MIC values for all of tested N-AgNPs samples are in the range from 4 to 64 μ g/ml. Minimal Bactericidal Concentrations (MBC) of studied N-AgNPs are equal to the values determined as MICs. We have not observed any bacterial growth on MH agar plates inoculated with residues from probes corresponding to MIC. It must be highlighted that in contrast to the majority of reported data MICs are not expressed as silver concentration but as concentration of the synthesized materials.

Table 5 MIC and MBC values of N-AgNPs.^a Results of three separate experiments are presented; no differences were noticed among experiments.

Bacterial strain	MIC and MBC [μ g/ml] ^b				
	AI24RT	AI24RTH	AI2HH(+5)	AI2HH(-5)	AR2HH(-5)
<i>E. coli</i> ATCC 23546	32	64	12	8	8
<i>P. aeruginosa</i> ATCC 10145	16	16	8	4	4
<i>K. pneumoniae</i> ATCC 13886	12	12	8	4	4
<i>S. aureus</i> ATCC 29213	32	64	12	12	12
<i>S. epidermidis</i> ATCC 12228	16	24	4	4	4

^a contents of silver in the studied materials are given in Fig. 9; ^b solution of the highest used concentration of DMSO (4% v/v) and DiSS (128 μ g/ml) were used as the control samples and they do not affect the normal growth of bacteria.

Cite this: DOI: 10.1039/c0xx00000x

www.rsc.org/xxxxxx

ARTICLE TYPE

As can be seen in Fig. 9 silver content in the samples determined on the basis of TGA is within the range 70-80%, with the exception of sample AI24RT in which the content of silver is only 22%. The very low concentration of silver in this sample indicates the presence of multilayer of organic molecules on the silver surface. As it can be seen in Table 5, different strength of antibacterial activity shown by the particular samples is not only a result of silver content.

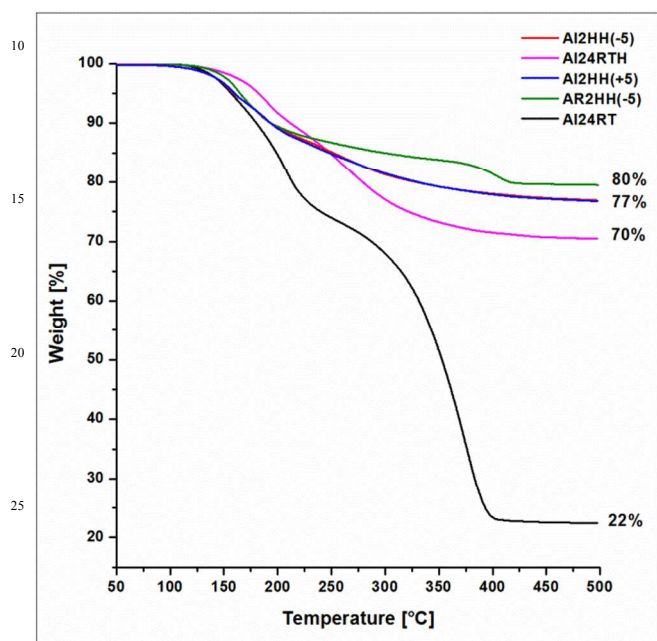


Fig. 9 Thermogravimetric (TG) curves of N-AgNPs and the determined silver content.

According to physicochemical properties of each sample described earlier it can be pointed out that AI2HH(-5) and AR2HH(-5), containing the smallest spherical nanoparticles with the narrowest size distribution (see Fig. 1), show the highest biocidal activity. The MICs values determined for these samples are significantly lower than those reported in literature for thiolate-capped AgNPs with similar size and slightly higher polydispersity (i.e. $7 \text{ nm} \pm 4 \text{ nm}$) to those in sample AR2HH(-5) in case of *E. coli* ($15 \mu\text{g/ml}$)¹⁵ and dramatically lower for *S. aureus* ($180 \mu\text{g/ml}$).¹⁵ To the best of our knowledge, activity of any thiolate-capped AgNPs against *P. aeruginosa*, *K. pneumoniae* and *S. epidermidis* has not been reported yet. Jain *et al.* have demonstrated the activity of AgNPs with wide size distribution ($6.0 \text{ nm} - 44 \text{ nm}$) against *P. aeruginosa* and *S. epidermidis* with $\text{MBC} = 12.5 \mu\text{g/ml}$ (expressed as silver concentration).⁵⁹

Panáček *et al.* have reported the activity of AgNPs against *K. pneumoniae* (ESBL-positive) with MBC in the range $6.7 \mu\text{g/ml}$ (for the nanoparticles with average size $25 \pm 8 \text{ nm}$ in diameter) to $54 \mu\text{g/ml}$ (for the nanoparticles with average size $35 \pm 11 \text{ nm}$ in

diameter) also expressed as silver concentration.⁶⁰ So, it can be concluded that the N-AgNPs synthesized under optimal reaction conditions exhibit (AR2HH(-5)) - the smallest sized particles) an excellent bactericidal activity towards both Gram-negative and Gram-positive strains. The least susceptible bacterial strain was *S. aureus*, which growth was inhibited at concentration of $12 \mu\text{g/ml}$ N-AgNPs. It has been reported that nanosilver exhibits more pronounced antibacterial activity towards Gram-negative species.^{7b} Also in our study Gram-negative species were more susceptible to analysed samples than *S. aureus*.

On the other hand, the samples AI24RT and AI24RTH containing the biggest particles (with size in range $20 - 120 \text{ nm}$ in diameter), and even aggregates, inhibited bacterial growth only in concentrations higher than $12 \mu\text{g/ml}$. This observation concerning the relation between the size and the biocidal activity stands in line with results described in earlier reports.¹¹ However, taking into account large size and high polydispersity of nanoparticles in these two samples, MICs values are relatively low. So, our results indicate that the nitroxide coverage of silver nanoparticles favours their antibacterial activity. In our opinion, it is most likely that the nitroxides covering silver surface may be oxidized under influence of ROS to positively charged oxoammonium ions (Eq.1), which are capable of strong interaction with negatively charged bacterial membrane leading to its physical damage and probable chemical modifications. It has been reported recently, by Bonilla-Cruz research group, that the hydroxyl groups attached to the surface of graphene oxide can be oxidized to ketone groups, whereas carboxylic groups can be transformed to alkoxyamine species under influence of oxoammonium cations.⁵⁴ The bacterial cell wall consists mainly of peptidoglycan containing many hydroxyl and carboxyl groups, and the oxidation of these groups under the influence of oxoammonium cations may lead to the structural changes and consequently loss of its functionality.

It is also worth mentioning that further experiments have shown a strong antifungal activity of N-AgNPs (data not shown). Subsequent studies are currently in progress.

4. Conclusion

The silver nanoparticles covered with nitroxides (N-AgNPs) have been successfully synthesized by one-phase procedure using bisnitroxide disulphide as capping ligand, DMF as reaction medium and solvent for reducing agent (NaBH_4). Effects of reaction conditions on the synthesis were studied. We have observed that the lowering of molar ratio of NaBH_4 to Ag^+ as well as its dropping velocity to the reaction mixture combined with decrease in reaction temperature significantly improve size distribution of the obtained silver nanoparticles. The N-AgNPs obtained under optimal reaction conditions are spherical, nearly uniformly distributed ($6.79 \pm 1.51 \text{ nm}$), devoid of Ag^+ impurities and long-term air stable. Similarly to other thiolate-capped silver

and gold nanoparticles, they can be repeatedly isolated and redissolved and characterized in solid state. FTIR and XPS confirmed functionalization of silver surface with nitroxide used in the synthesis and showed the presence of intact disulphide bonds in organic layer. On the basis of the ESR spectra simulations and quantitative data from the XPS analysis it was estimated that ca. 8% of ligands (biradicals) are attached by disulphide groups adsorbed on the surface, ca. 90 % of ligands is attached to the silver surface as thiolate moieties and ca. 1-2% are linked via Ag-O bonds formed between unpaired electrons of nitroxides and conduction electrons from the silver surface.

The synthesized N-AgNPs exhibit high antimicrobial activity towards both Gram-negative (*E. coli*, *P. aeruginosa*, *K. pneumoniae*) and Gram-positive strains (*S. aureus*, *S. epidermidis*). The determined MICs values for the sample obtained under optimal reaction conditions are very low in comparison with these reported earlier for other thiolate-capped silver nanoparticles and range from 4 µg/ml (against *P. aeruginosa*) to 12 µg/ml (against *S. aureus*).

Due to the combination of nitroxides and nanosilver, the synthesized material may find, besides biocidal applications, numerous others in catalysis, organic synthesis, polymer chemistry, biochemical studies and material science.

Acknowledgements

This work has been supported by Project DEC-2011/01/B/ST5/03941 from National Science Center.

TEM images have been obtained using the equipment purchased within CePT Project No.: POIG.02.02.00-14-024/08-00.

XPS analysis have been performed using the equipment of Mazovia Center for Surface Analysis in Institute of Physical Chemistry PAS.

Notes and references

^aUniversity of Warsaw, Faculty of Chemistry, Pasteura 1, 02-093 Warsaw, Poland

^bUniversity of Warsaw, Faculty of Biology, Institute of Microbiology, Department of Bacterial Genetics, Miecznikowa 1, 02-096 Warsaw, Poland

^cMedical University of Warsaw, Faculty of Pharmacy with the Laboratory Medicine Division, Banacha 1, 07-097 Warsaw, Poland

† Electronic Supplementary Information (ESI) available: ESR spectrum of DiSS, general survey XPS spectrum of DiSS and N-AgNPs, EDS spectrum of N-AgNPs, UV-vis spectra of solution of N-AgNPs after a given period of time, quantitative results of XPS analysis of DiSS, calculations of the surface density of DiSS (sample AR2HH(-5)). See DOI:10.1039/b000000x/

References

- M. A. Shenashen, S. A. El-Safy, E. A. Elshehy, *Part. Part. Syst. Charact.*, 2014, **31**, 293-316 and references therein.
- a. U. Kreibitz and M. Vollmer, "Optical properties of metal clusters", Springer, Berlin, 1995; b. C.F. Bohren, D.R. Huffman "Absorption and scattering of light by small particles", 1983, Wiley, New York; c. P. K. Jain, X. Huang, I. H. El-Sayed, M. A. El-Sayed, *Plasmonics*,

- 2007, **2**, 107-118; d. T. Huang, X-H., N. Xu, *J. Mater. Chem.*, 2010, **20**, 9867-9876.
- K-S. Lee, M. A. El-Sayed, *J. Phys. Chem. B*, 2006, **110**, 19220-19225.
- X. Le Guével, C. Spies, N. Daum, G. Jung, M. Schneider, *Nano. Res.*, 2012, **5**, 379-387.
- A. R. Tao, D. P. Ceperley, P. Sinsersuksakul, A. R. Neureuther, P. Yang, *Nano Lett.*, 2008, **8**, 4033-4038.
- Y. Wang, B. Yan, L. Chen, *Chem. Rev.*, 2013, **113**, 1391-1428.
- a. S. Chernousova, M. Epple, *Angew. Chem. Int. Ed.*, 2013, **52**, 1636-1653; b. L. Rizzello, P. P. Pompa, *Chem. Soc. Rev.*, 2014, **43**, 1501-1518; c. Q. H. Tran, V. Q. Nguyen, A-T Le, *Adv. Nat. Sci. Nanosci. Nanotechnol.*, 2013, **4**, 033001-0330020; d. M. J. Hajipour, K. M. Fromm, A. A. Ashkarran, D. J. de Aberasturi, I. R. de Larramendi, T. Royo, V. Serpooshan, W. J. Parak, M. Mahmoudi, *Trends Biotechnol.*, 2012, **30**, 499-511 and references therein.
- B. Nowack, H. F. Krug, M. Height, *Environ. Sci. Technol.*, 2011, **45**, 1177-1183.
- a. E. Hwang, J. Lee, Y. Chae, Y. Kim, B. Kim, B. Sang, M. Gu, *Small*, 2008, **7**, 746-750; b. A. B. Smetana, K. J. Klabunde, G. R. Marchin, C. M. Sorensen, *Langmuir*, 2008, **24**, 7457-7464.
- K. B. Holt, A. J. Bard, *Biochemistry*, 2005, **44**, 13214-13223.
- O. Choi, Z. Hu, *Environ. Sci. Technol.*, 2008, **42**, 4583-4588.
- S. Pal, Y. K. Tak, J. M. Song, *Appl. Environ. Microbiol.*, 2007, **73**, 1712-1720.
- A. M. El Badawy, R. G. Silva, B. Morris, K. G. Scheckel, M. T. Suidam, T. M. Tolaymat, *Environ. Sci. Technol.*, 2011, **45**, 283-287.
- S. Y. Kang, K. Kim, *Langmuir*, 1998, **14**, 226-230.
- E. Amato, Y. A. Diaz-Fernandez, A. Taglietti, P. Pallavicini, L. Pasotti, L. Cucca, C. Milanese, P. Grisoli, C. Dacarro, J. M. Fernandez-Hechavarria, V. Necchi, *Langmuir*, 2011, **27**, 9165-9173.
- a. A. Taglietti, Y. A. Diaz-Fernandez, E. Amato, L. Cucca, G. Dacarro, P. Grisoli, V. Necchi, P. Pallavicini, L. Pasotti, M. Patrini, *Langmuir*, 2012, **28**, 8140-8148.
- A. Taglietti, Y. A. Diaz Fernandez, P. Galinetto, P. Grisoli, C. Milanese, P. Pallavicini, *J. Nanopart. Res.*, 2013, **15**, 1-13.
- P. Graf, A. Manton, A. Foelske, A. Shkilnyy, A. Mašić, A. F. Thünemann, A. Taubert, *Chem-Eur J.*, 2009, **15**, 5831-5844.
- L. Tebben, A. Studer, *Angew. Chem. Int. Ed.*, 2011, **50**, 5034-5068.
- R. Ciriminna, G. Palmisano, M. Pagliaro, *ChemCatChem*, 2015, **7**, 552-558.
- J. Nicolas, Y. Guillauneuf, C. Lefay, D. Bertin, D. Gignes, B. Charleux, *Prog. Polym. Sci.*, 2013, **38**, 63-235.
- L. J. Berliner ed. "Spin labeling: theory and applications." Academic Press, 2013.
- N. M. Gallagher, A. Olankitwanit, A. Rajca, *J. Org. Chem.*, 2015, **80**, 1291-1298.
- G. I. Likhtenshtein, J. Yamauchi, S. Nakatsuji, A. I. Smirnov, R. Tamura, "Nitroxides Applications in Chemistry, Biomedicine and Materials Science", Wiley-VCH, Weinheim, 2008.
- B. P. Soule, F. Hyodo, K. Matsumoto, N. L. Simone, J. A. Cook, M. C. Krishna, J. B. Mitchell, *Free Rad. Biol. Med.*, 2007, **42**, 1632-1650.
- A. Kaim, J. Szydłowska, P. Piotrowski, E. Megiel, *Polyhedron*, 2012, **46**, 119-123.
- O. Swiech, R. Bilewicz, E. Megiel, *RSC Adv.*, 2013, **3**, 5979-5986.
- K. Zawada, W. Tomaszewski, E. Megiel, *RSC Adv.*, 2014, **4**, 23876-23885.
- R. Nicolay, L. Marx, P. Hemery, K. Matyjaszewski, *Macromolecules* 2007, **40**, 9217-9223.
- Clinical and Laboratory Standards Institute, Approved standard M7-A9, Methods for dilution antimicrobial susceptibility tests for bacteria that grow aerobically. 9th ed. CLSI, Wayne, Pa, 19087 USA (2012).
- A. Mari, P. Imperatori, G. Marchegiani, L. Pilloni, A. Mezzi, S. Kaciulis, C. Cannas, C. Meneghini, S. Mobilio, L. Suber, *Langmuir*, 2010, **26**, 15561-15566.
- B. A. Korgel, S. Fullam, S. Connolly, D. Fitzmaurice, *J. Phys. Chem. B*, 1998, **102**, 8379-8388.

- ³³ M. D. Porter, T. B. Bright, D. L. Allara, C. E. D. Chidsey, *J. Am. Chem. Soc.*, 1987, **109**, 3559-3568.
- ³⁴ A. Kaim, E. Megiel, *J. Polym. Sci. Part A: Polym. Chem.*, 2005, **43**, 1827-1844.
- ³⁵ P. Ionita, A. Caragheorgheopol, B.C. Gilbert, V. Chechik, *J. Phys. Chem. B*, 2005, **109**, 3734-3742.
- ³⁶ V. Chechik, H. J. Wellsted, A. Korte, B. C. Gilbert, H. Caldararu, P. Ionita, A. Caragheorgheopol, *Faraday Discuss.*, 2004, **125**, 279-291.
- ³⁷ A.H. Goldberg, D.A. Dougherty, *J. Am. Chem. Soc.*, 1983, **105**, 284-290.
- ³⁸ E. G. Rozantzev, M. B. Neiman, *Tetrahedron*, 1964, **20**, 131-137.
- ³⁹ R. Owenius, M. Engström, M. Lindgren, M. Huber, *J. Phys. Chem. A*, 2001, **105**, 10967-10977.
- ⁴⁰ P. Ionita, A. Caragheorgheopol, B.C. Gilbert, V. Chechik, *J. Am. Chem. Soc.*, 2002, **124**, 9048-9049.
- ⁴¹ Z. Deng, M. Chen, L. Wu, *J. Phys. Chem. C*, 2007, **111**, 11692-11698.
- ⁴² J. F. Moulder, W. F. Stickle, P. E. Sobol, K. D. Bomben, *Handbook of X-ray Photoelectron Spectroscopy*, Eden Prairie, Minn.:Perkin-Elmer Corporation, Physical Electronics, 1992.
- ⁴³ I. Lopez-Salido, D. C. Lim, Y. D. Kim, *Surf. Sci.*, 2005, **588**, 6-18.
- ⁴⁴ A. I. Boronin, S. V. Koscheev, G. M. Zhidomirov, *J. Electron. Spectrosc. Relat. Phenom.*, 1998, **96**, 43-51.
- ⁴⁵ NIST X-ray Photoelectron Spectroscopy Database, Standard Reference Database 20, Version 4.1, data compiled and evaluated by A.V. Naumkin, A. Kraut-Vass, S. W. Gaarenstroom, C. J. Powell, last updated 2012.
- ⁴⁶ O. Swiech, N. Hryniewicz-Sudnik, B. Palys, A. Kaim, R. Bilewicz, *J. Phys. Chem. C*, 2011, **115**, 7347-7354.
- ⁴⁷ H. Schönherr, H. Ringsdorf, *Langmuir*, 1996, **12**, 3891-3897.
- ⁴⁸ M. E. Castro, L. A. Pressley, J. M. White, *Surf. Sci.*, 1991, **256**, 227-241.
- ⁴⁹ J. C. Munro, C. W. Frank, *Polymer*, 2003, **44**, 6335-6344.
- ⁵⁰ D. G. Castner, K. Hinds, D. W. Grainger, *Langmuir*, 1996, **12**, 5083-5086.
- ⁵¹ L. A. Porter, Jr., D. Ji, S. L. Westcott, M. Graupe, R. S. Czermuszewicz, N. J. Halas, T. R. Lee, *Langmuir*, 1998, **14**, 7378-7386.
- ⁵² E. Lopez-Tobar, B. Hernandez, M. Ghomi, S. Sanchez-Cortes, *J. Phys. Chem. C*, 2013, **117**, 1531-1537.
- ⁵³ K. Haubner, J. Murawski, P. Olk, L. M. Eng, C. Ziegler, B. Adolphi, E. Jaehne, *ChemPhysChem*, 2010, **11**, 2131-2139.
- ⁵⁴ Y. I. Avila-Vega, C. C. Leyva-Porras, M. Mireles, M. Quevedo-Lopez, J. Macossay, J. Bonilla-Cruz, *Carbon*, 2013, **63**, 376-389.
- ⁵⁵ K. Endo, C. Inoue, N. Kobayashi, M. Aida, *J. Phys. Chem. Solids*, 1994, **55**, 471-478.
- ⁵⁶ M. J. Hostetler, J. E. Wingate, C-J. Zhong, J. E. Harris, R. W. Vachet, M. R. Clark, J. D. Londono, S. J. Green, J. J. Stokes, G. D. Wignall, G. L. Glish, M. D. Porter, N. D. Evans, R. W. Murray, *Langmuir*, 1998, **14**, 17-30.
- ⁵⁷ H. Hinterwirth, S. Kappel, T. Waitz, T. Prohaska, W. Lindner, M. Lämmerhofer, *ACS Nano*, 2013, **7**, 1129-1136.
- ⁵⁸ M. D. Torelli, R. A. Putans, Y. Tan, S. E. Lohse, C. J. Murphy, R. Hamers, *ACS Appl. Mater. Interfaces*, 2015, **7**, 1720-1725.
- ⁵⁹ J. Jain, S. Arora, J. M. Rajwade, P. Omay, S. Khandelwal, K. M. Paknikar, *Mol. Pharm.*, 2009, **6**, 1388-1401.
- ⁶⁰ A. Panáček, L. Kvítek, R. Prucek, M. Kolář, R. Večeřova, N. Pizúrová, V. K. Sharma, T. Nevěčna, R. Zbořil, *J. Phys. Chem. B*, 2006, **110**, 16248-16253.